AFRL-AFOSR-VA-TR-2024-0139

High Power Fiber Lasers Utilizing Intermodal Nonlinearities

Ramachandran, Siddharth
TRUSTEES OF BOSTON UNIVERSITY
1 SILBER WAY
BOSTON, MA, 02215
USA

01/30/2024
Final Technical Report

Air Force Research Laboratory
Air Force Office of Scientific Research
Arlington, Virginia 22203
Air Force Materiel Command

REPORT DOCUMENTATION PAGE

PLEASE DO NOT RETURN YOUR FORM TO THE ABOVE ORGANIZATION.

1. REPORT DATE	2. REPORT TYPE	3. DATES COVERED	
20240130	Final	START DATE 20140901	END DATE 20210831

4. TITLE AND SUBTITLE
High Power Fiber Lasers Utilizing Intermodal Nonlinearities

5a. CONTRACT NUMBER	5b. GRANT NUMBER	5c. PROGRAM ELEMENT NUMBER
	FA9550-14-1-0165	61102F
5d. PROJECT NUMBER	**5e. TASK NUMBER**	**5f. WORK UNIT NUMBER**

6. AUTHOR(S)
Siddharth Ramachandran

7. PERFORMING ORGANIZATION NAME(S) AND ADDRESS(ES)
TRUSTEES OF BOSTON UNIVERSITY
1 SILBER WAY
BOSTON, MA 02215
USA

8. PERFORMING ORGANIZATION REPORT NUMBER

9. SPONSORING/MONITORING AGENCY NAME(S) AND ADDRESS(ES)	10. SPONSOR/MONITOR'S ACRONYM(S)	11. SPONSOR/MONITOR'S REPORT NUMBER(S)
Air Force Office of Scientific Research 875 N. Randolph St. Room 3112 Arlington, VA 22203	AFRL/AFOSR RTB1	AFRL-AFOSR-VA-TR-2024-0139

12. DISTRIBUTION/AVAILABILITY STATEMENT
A Distribution Unlimited: PB Public Release

13. SUPPLEMENTARY NOTES

14. ABSTRACT
The goal of this BRI program is the investigation of novel nonlinear effects and phenomena by (1) exploiting the higher dimensional design space afforded by higher order modes (HOM) in fibers, as well as the subset of such modes that carry orbital angular momentum (OAM), and (2) enable nonlinear fiber optics at high pulse energies, currently critically limited by the low power handling constraints of photonic crystal fibers. Applications range from underwater communications and sensing to quantum encryption and imaging. Unlike in crystals, parametric processes in optical fibers exploit the third order (3)nonlinearity, which need phase matching to be efficient. In a single-mode system, phase matching is obtained by control of the chromatic dispersion of an optical fiber; specifically it requires that the zero-dispersion of the medium or waveguide be spectrally proximal to the pump wavelength. To achieve this at user-defined pump wavelengths, especially in the visible or near-IR spectral range, a fundamental requirement is for the mode area to be decreased in Silica-based fibers (other fiber materials have, to date, not been shown to be stable enough to be viable as high-power hosts). This can be readily achieved with photonic crystal waveguides and fibers, but this methodology yields color-tunability at the expense of pulse energy, since mode area has to be continually decreased as the pump wavelength decreases. In this program, we leveraged recent advances in optical fibers, which showed that sufficiently high order HOMs are stable, even over lengths exceeding km. As such, a multimode fiber (MMF) platform provides for a countably infinite number of select (but not all) spatial modes that do not uncontrollably mix, yielding mode distortions and speckle patterns that have been considered unavoidable in MMFs. This allows for efficient nonlinear optics in MMFs because the interaction lengths are effectively the length of fiber one chooses to use, rather than the stochastically determined mode-coupling length. This provides four key benefits: (1) the dispersion zero decreases with mode order, whereas the mode area is simply governed by waveguide size – hence this breaks the tradeoff between mode-area (and, thus, power-handling capability); (2) phase matching could be achieved via intermodal interactions, which no longer forces a dispersion constraint on any mode, opening up the design space, considerably; (3) angular momentum conservation laws provide a novel means to control nonlinear interactions, including effects such as chirality induced tailoring of Brillouin and Raman scattering; and (4) group velocity diversity amongst modes yields selective ultrashort pulse interactions not seen in bulk media or single mode fibers. The primary achievements in the course of this program are listed below.

15. SUBJECT TERMS

16. SECURITY CLASSIFICATION OF:			17. LIMITATION OF ABSTRACT	18. NUMBER OF PAGES
a. REPORT	b. ABSTRACT	c. THIS PAGE		
U	U	U	UU	13

19a. NAME OF RESPONSIBLE PERSON	19b. PHONE NUMBER *(Include area code)*
JOHN LUGINSLAND	000-0000

Standard Form 298 (Rev.5/2020)
Prescribed by ANSI Std. Z39.18

AFOSR: FA9550-14-1-0165:
Project Title: BRI: High-power fiber lasers using intermodal nonlinearities

PI: Siddharth Ramachandran,
Distinguished Professor of Engineering,
Boston University
+1-617-353-9881; sidr@bu.edu;
https://sites.bu.edu/ramachandranlab/

Abstract: The goal of this BRI program is the investigation of novel nonlinear effects and phenomena by (1) exploiting the higher dimensional design space afforded by higher order modes (HOM) in fibers, as well as the subset of such modes that carry orbital angular momentum (OAM), and (2) enable nonlinear fiber optics at high pulse energies, currently critically limited by the low power handling constraints of photonic crystal fibers. Applications range from underwater communications and sensing to quantum encryption and imaging. Unlike in crystals, parametric processes in optical fibers exploit the third order $\chi^{(3)}$nonlinearity, which need phase matching to be efficient. In a single-mode system, phase matching is obtained by control of the chromatic dispersion of an optical fiber; specifically it requires that the zero-dispersion of the medium or waveguide be spectrally proximal to the pump wavelength. To achieve this at user-defined pump wavelengths, especially in the visible or near-IR spectral range, a fundamental requirement is for the mode area to be decreased in Silica-based fibers (other fiber materials have, to date, not been shown to be stable enough to be viable as high-power hosts). This can be readily achieved with photonic crystal waveguides and fibers, but this methodology yields color-tunability at the expense of pulse energy, since mode area has to be continually decreased as the pump wavelength decreases. In this program, we leveraged recent advances in optical fibers, which showed that sufficiently high order HOMs are stable, even over lengths exceeding km. As such, a multimode fiber (MMF) platform provides for a countably infinite number of select (but not all) spatial modes that do not uncontrollably mix, yielding mode distortions and speckle patterns that have been considered unavoidable in MMFs. This allows for efficient nonlinear optics in MMFs because the interaction lengths are effectively the length of fiber one chooses to use, rather than the stochastically determined mode-coupling length. This provides four key benefits: (1) the dispersion zero decreases with mode order, whereas the mode area is simply governed by waveguide size – hence this breaks the tradeoff between mode-area (and, thus, power-handling capability); (2) phase matching could be achieved via *inter*modal interactions, which no longer forces a dispersion constraint on any mode, opening up the design space, considerably; (3) angular momentum conservation laws provide a novel means to control nonlinear interactions, including effects such as chirality induced tailoring of Brillouin and Raman scattering; and (4) group velocity diversity amongst modes yields selective ultrashort pulse interactions not seen in bulk media or single mode fibers. The primary achievements in the course of this program are listed below.

1) Demonstration of intermodal FWM across two octaves

We demonstrated[1] intermodal FWM, and associated coherent spectral translations over two octaves (400–1700 nm) and 11 interacting spatial modes ($LP_{0,6}$–$LP_{0,16}$), using azimuthally symmetric fiber modes that behave like Bessel beams (Fig. 1). We show that this uniquely stable set of modes offers a variety of momentum conservation paths, akin to angle control in bulk nonlinear crystals. The primary reason for the wide spectral translation and the ability to

cascade through so many modes was the use of modes in an MMF that are exceptionally stable, implying that their nonlinear interactions are far more efficient that those attempted with conventional MMFs in the past, where mode instability acts as an effective decoherer. Thus, intermodal nonlinearities with Bessel beams in fibers may enable truly monolithically integrated nonlinear-optical devices that combine the advantages of the bulk and guided-wave worlds. The significance of this experimental result led to our manuscript on this topic being chosen as the cover article of the high impact journal by OSA, *Optica* (see cover image on previous page).

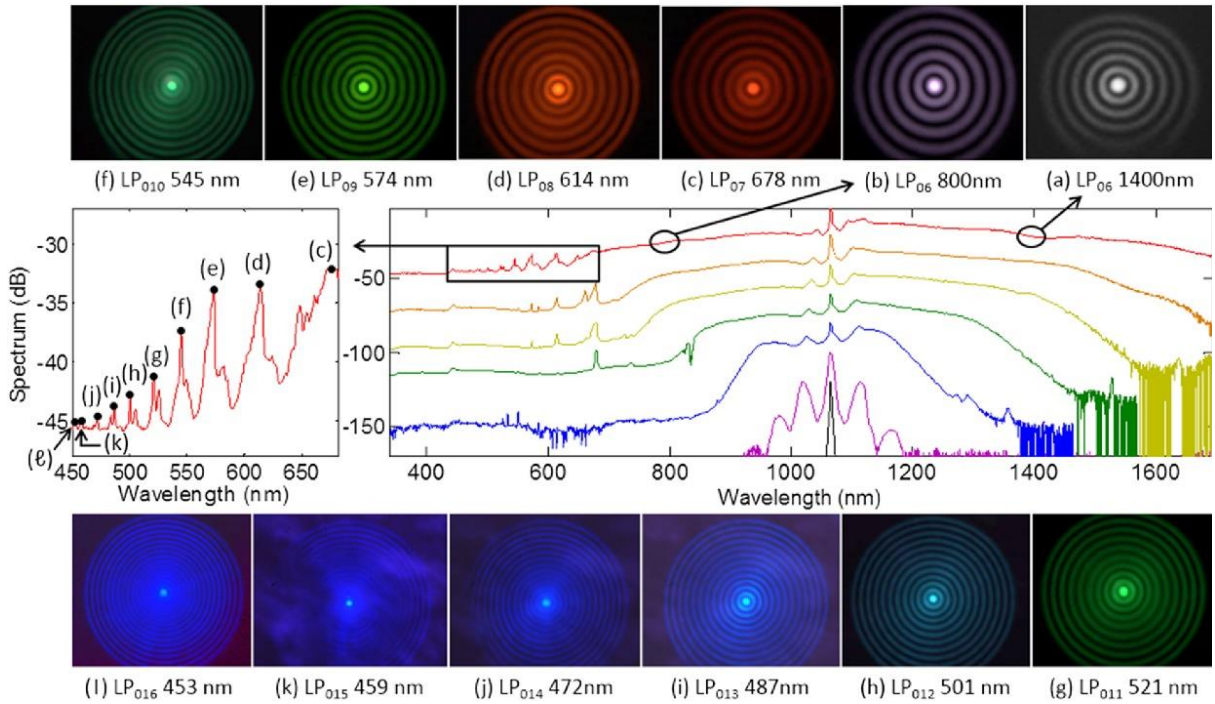

Fig. 1. Output spectra and mode images from intermodal FWM. Red, topmost spectrum was obtained with a fiber of length 16.3 m; lower spectra correspond to 10.3, 8.3, 6.3, 4.3, 2.3, and 1.3 m fiber lengths, respectively (offset for clarity), for 34.7 kW of input peak power. Left inset spectrum is a zoomed-in view of the 16.3 m spectrum, highlighting intermodal peaks in the visible region. Mode images are shown for representative portions of the continuum spectrum [(a) and (b)], and each of the discrete peaks [(c)–(l)]. Between 700 and 1400 nm, the mode remains $LP_{0,6}$; each of the discrete peaks in the visible corresponds to $LP_{0,m}$ modes of increasing radial order.

2) <u>High-power sources at non-traditional wavelengths via seeded intermodal FWM:</u>

Given the plethora of phase-matching possibilities, and hence ability to obtain spontaneous emission in a large range of wavelengths, we tested the ability to seed the process – i.e. add a low-power source at the input of the fiber at a wavelength and mode corresponding to either one of a pair of Stokes and anti-Stokes wavelengths in a FWM process – to investigate the gain and power-scalability that such an MMF platform provides. We illustrate the versatility of this approach by demonstrating fiber-optic parametric amplifier (FOPA) sources[2]. As Fig. 2 shows, when the MMF is pumped with the $LP_{0,7}$ mode, the fiber output yields ~300 ps pulses with emission wavelengths of 974 and 1173 nm, respectively, corresponding to the vital blue/green and yellow portions of the visible spectrum (via Second Harmonic Generation). The on-off gain of these FOPAs exceeds 50 dB, enabling the aforementioned pulses to have peak powers of ~15 kW (Fig. 3). With peak pump depletion values exceeding 70%, this platform is an efficient means to generate high-power pulses at colors not typically accessible by conventional high-power fiber lasers and amplifiers.

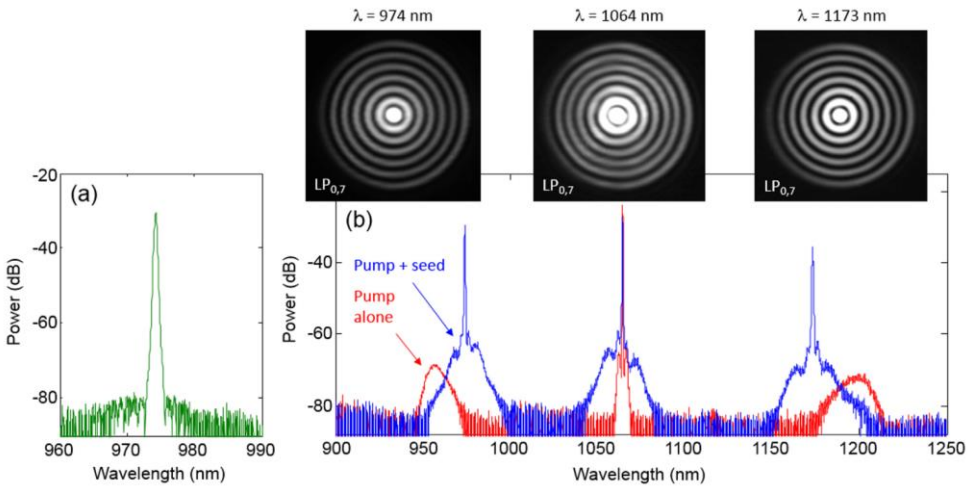

Fig. 2. (a) Seed spectrum and (b) output spectra for FOPA source A; spectrally filtered mode images for the anti-Stokes, pump, and Stokes waves are shown inset – all in $LP_{0,7}$ as expected.

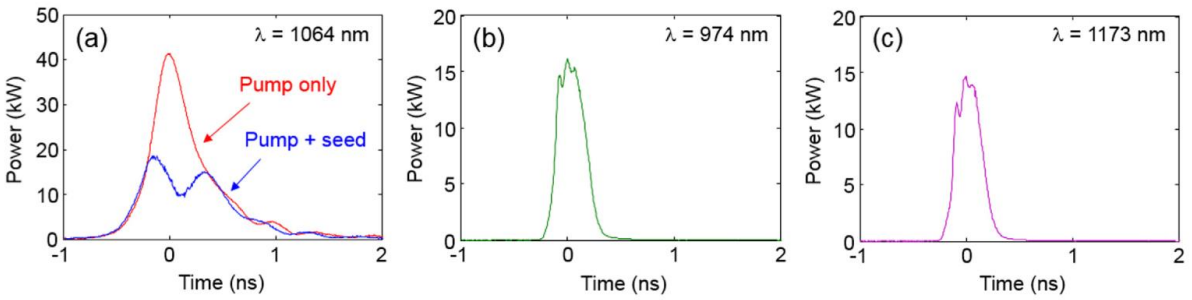

Fig. 3. (a) Pump pulse temporal profiles with (blue) and without (red) the seed; Measured anti-Stokes (b) and Stokes (c) pulse with 64-point running average.

While we have, thus far, described the utility of Bessel beam-like $LP_{0,m}$ modes of MMFs for achieving FWM-based frequency translation, even further selectivity and control may be obtained by exploiting angular momentum selection rules for FWM. For fiber modes carrying orbital angular momentum (OAM), the overlap integral that specifies the strength of FWM interactions is non-zero only when OAM is conserved amongst the four participating photons. Hence, OAM conservation rules additionally provide selectivity, which ensures that the emission is only in the spectral line(s) one desires. As an example, we showed the first generation of kW peak power 888-nm light in a high OAM state[3]. Nonlinear frequency generation of light-carrying orbital angular momentum (OAM), which facilitates realization of on-demand, frequency-diverse optical vortices, would have utility in fields such as super-resolution microscopy, space-division multiplexing and high-dimensional quantum entanglement. The significance of these results is evident with the selection of the article as the cover art for the January 2020 issue of *APL Photonics* (Fig. 4) as well as its contents being highlighted as a *SciLight* item with editorial comments.

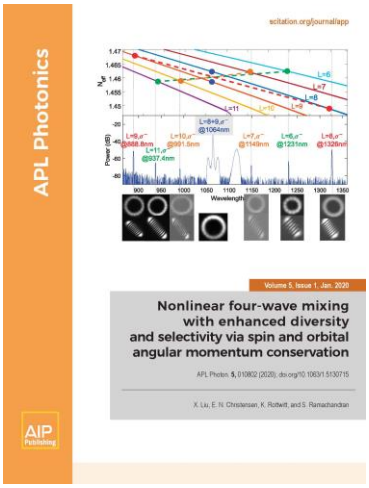

Fig. 4. Cover art of representative OAM FWM spectra in Jan. 2020 issue of *APL Photonics*.

3) Power-scalable & broadband frequency conversion for wavelength-tunable sources:

One significant drawback of intermodal FWM schemes described above has been the narrow-band nature of these interactions. We have shown how phase *and* group-velocities of modes may be engineered to obtain broadband as well as wideband frequency conversion. Specifically, for Stokes and anti-Stokes pairs at which phase matching is satisfied *and* the group velocities of the respective participating modes are matched, one obtains broadband phase matching over bandwidths exceeding 60 nm. Then, seeding this process with a lower power wavelength tunable seed yields a wavelength-tunable high-power source. Figure 5 illustrates one such demonstration, which can coherently convert 15xx nm light into 7xx nm light with peak powers of ~10 kW, *and* the source is tunable[4]. Hence, this represents the demonstration of the first all-fiber version of a Ti:Sapphire laser with high power output. This result got significant attention upon publication, being chosen as the cover art article for the January 2019 issue of *Photonics Research*.

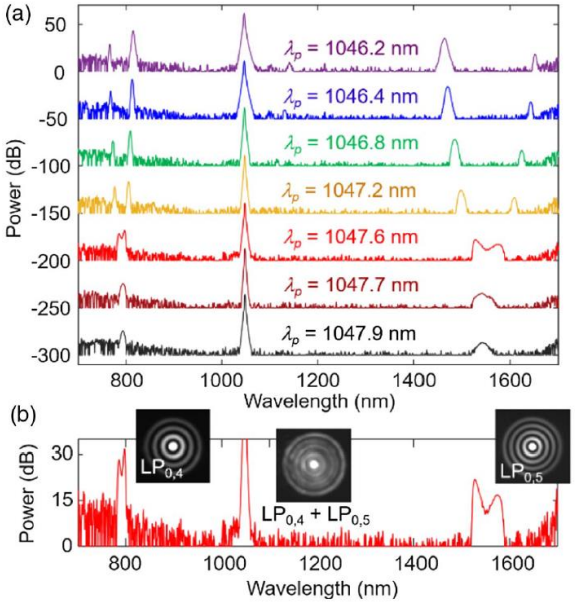

(c)

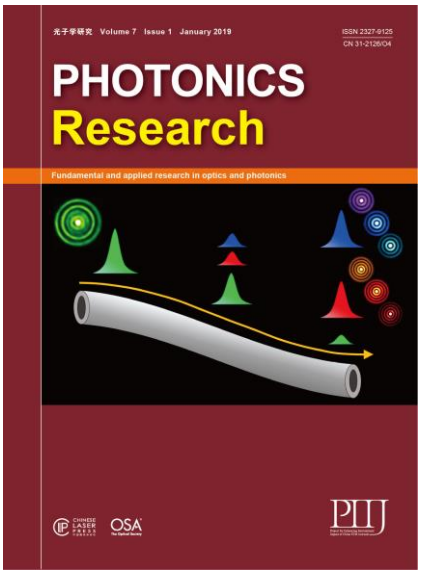

Fig. 5: (a) Spontaneous four-wave mixing spectra as a function of pump wavelength; each spectrum offset by 50 dB for clarity. (b) Zoom-in of the bandwidth-optimized spontaneous spectrum (λ_p = 1047.6 nm) with mode images inset. (c) Cover art image for January 209 issue of *Photonics Research*.

4) Super-continuum generation of vortex light:

We now turn our attention to nonlinear interactions with ultrashort (~100 fs) pulses, where self-phase modulation (SPM) plays a significant role, especially in the generation of coherent supercontinua. In bulk media, OAM beams primarily differ in spatial phase, so the nonlinear overlap integral for self-phase matched $\chi(3)$ processes remains the same across the 4-fold degenerate subspace of beams (formed by different combinations of spin and orbital angular momentum) carrying the same OAM magnitude. This indistinguishable nature of nonlinear coupling implies that supercontinuum generation, which substantially relies on self/cross-phase modulation, and Raman soliton shifting of ultrashort pulses, typically results in multimode outputs that do not conserve OAM. Using specially designed optical fibers that support OAM modes

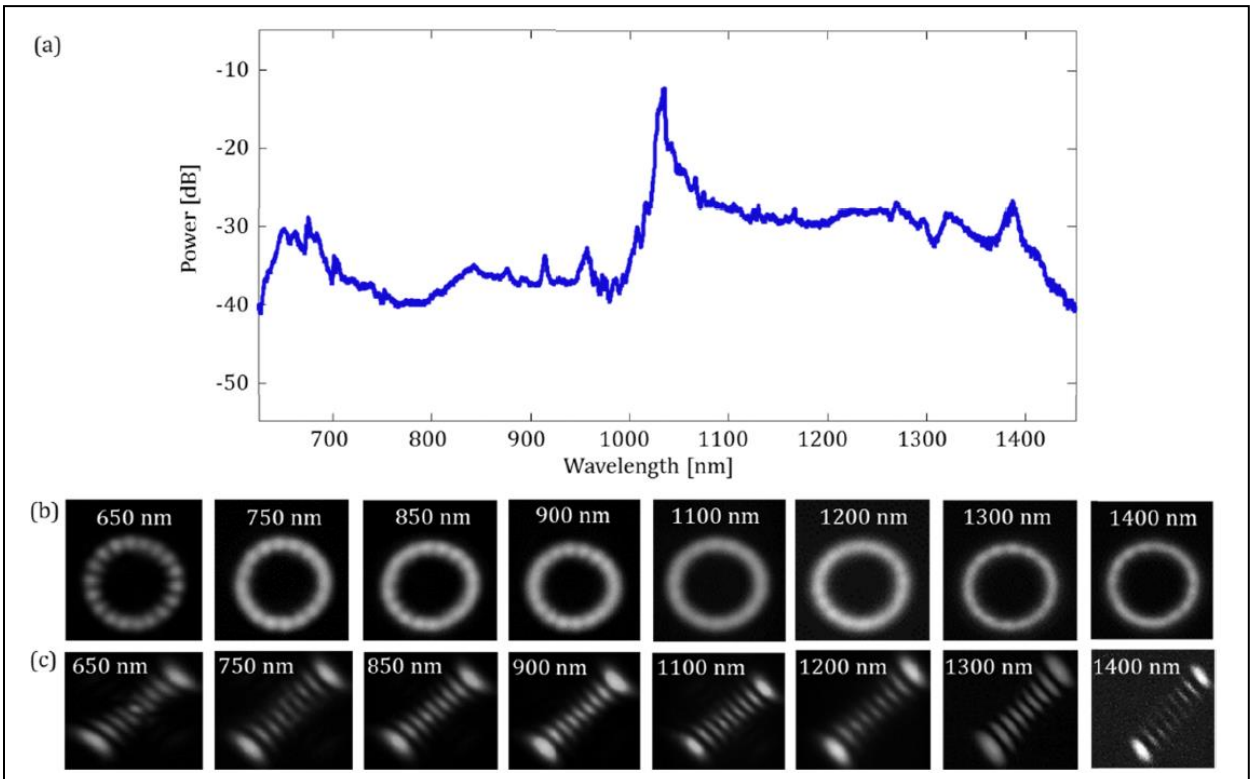

Fig. 6: (a) Measured supercontinuum spectra in the $\mathcal{L} = 8$ mode of air-core fiber. (b) Output mode images in the launched polarization at different wavelengths. (c) Hermite-Gaussian like mode images at different wavelengths of the supercontinuum, confirming that the launched OAM mode order ($\mathcal{L} = 8$) is maintained across the nonlinearly generated frequencies.

whose group velocity can be tailored, we demonstrate[5] Raman solitons in OAM modes as well as the first supercontinuum spanning more than an octave (630 nm to 1430 nm), with the entire spectrum in the same polarization as well as OAM state (Fig. 6). This is fundamentally possible because spin-orbit interactions in suitably designed fibers lead to large effective index and group velocity splitting of modes, and this helps tailoring nonlinear mode selectivity such that all nonlinearly generated frequencies reside in modes with high spatial mode purity. This work led to new insight on the propagation of superposition OAM states, which can be used to artificially tailor optical activity[6], resulting in a patent[7] for developing high-resolution wavemeters.

5) <u>Soliton Self-Mode Conversion (SSMC):</u>

SSMC is a new manifestation of Raman scattering of ultrashort (~100-fs) pulses that was first discovered in the course of this program[8]. It represents a unique nonlinear scattering pathway that enables wideband spectral tuning of highly energetic pulses, with peak powers exceeding the state of the art within a fiber by at least 10x. Figure 7 shows a fiber-cutback evolution of the process, and clearly indicates that the mode order switches, and all energy is transferred, each time a soliton in one mode is at a spectral position where it is group-velocity matched to another mode that is spectrally separated by approximately one Raman Stokes-shift. Practically, we demonstrate spectral coverage of energetic soliton pulses from 1000nm to 1700nm either by length or power tuning. Achieved pulse energies exceed 80 nJ for ~74-fs pulses, representing a peak power of ~ 1.1 MW.

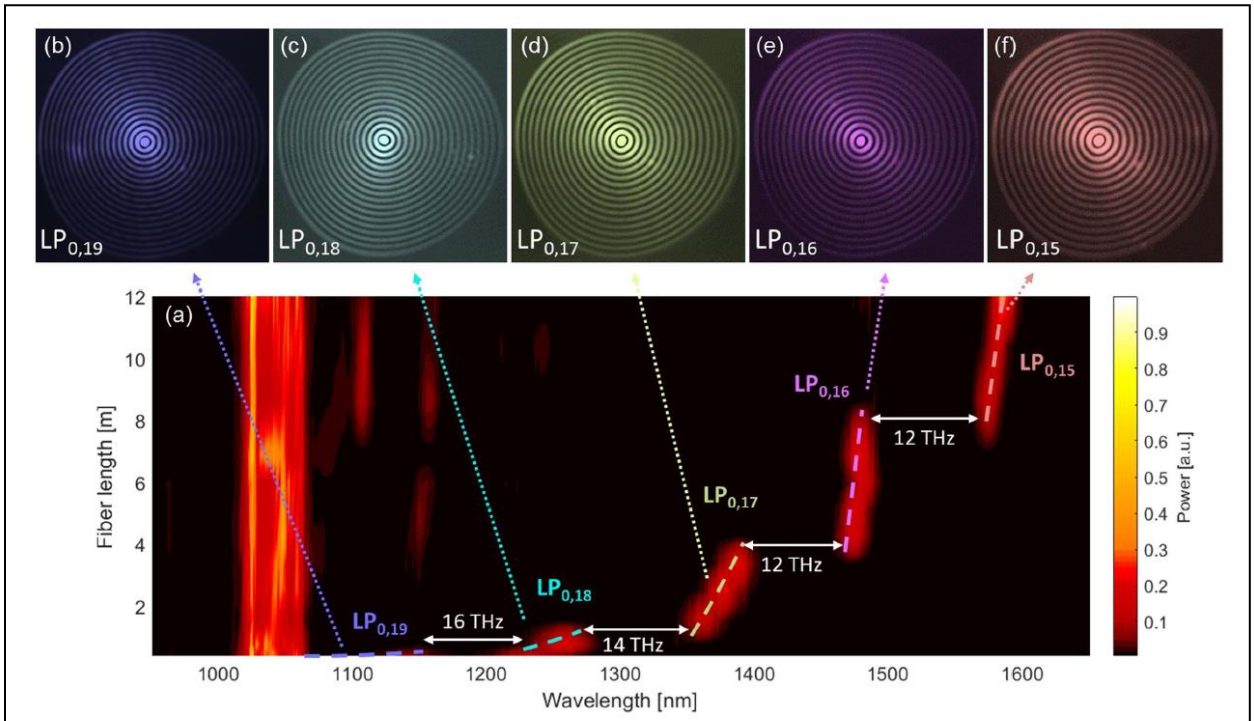

Fig. 7. (a) Spectra as a function of fiber length; the launched pulse at 1045 nm is in the LP0,19 mode. (b)–(f) Representative mode images taken using 10-nm bandpass filters of various spectral features.

From a fundamental standpoint, this nonlinearity subsumes even the concurrently competing seeded nonlinearity – the well-known process of soliton self-frequency shifting (SSFS). Theoretical simulations[9] predict that this phenomenon could initiate just from quantum shot noise alone, pointing both to the fundamental nature of this interaction as well as the unique physics it reveals, wherein a noise initiated process subsumes a seeded process. This theoretical prediction

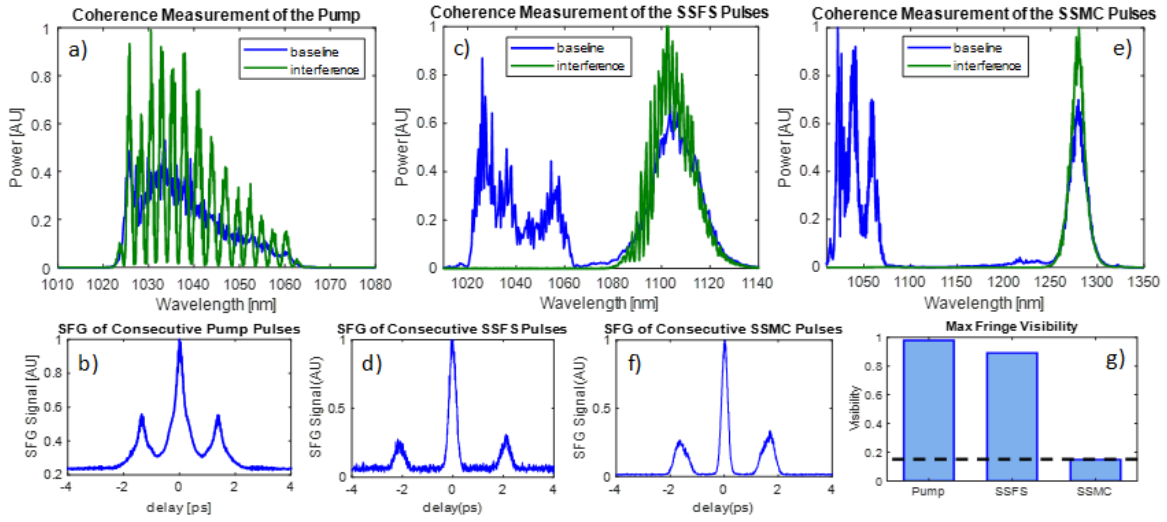

Fig. 8. The baseline spectra (when one of the interferometer arms is blocked) and the interference spectra for pump (a and b), SSFS (c and d) and SSMC (e and f) are provided. (a) Spectrum of the consecutive pump beams (b) SFG of the consecutive pump pulses (c) Spectrum of the consecutive SSFS beams (d) SFG of the consecutive SSFS pulses (e) Spectrum of the consecutive SSMC beams (f) SFG of the consecutive SSMC pulses (g) Maximum fringe visibility for pump, SSFS and SSMC cases.

was experimentally confirmed by performing shot-to-shot coherence measurements[10]. As shown in Fig. 8, whereas the pump and conventional frequency shifting Raman nonlinear processes maintain shot-to-shot coherence, the SSMC pulse completely loses this coherence, being quantum noise-photon initiated. Continued theoretical investigations of this phenomenon also point to a debilitating aspect of multimode nonlinear optics – conventional SSFS that typically maintains high coherence starts losing this coherence at the onset of SSMC[11]. This effect points to the fact that, while the SSMC pulses are themselves highly robust and useful for many applications, SSFS may, in fact, have spectral tunability limitations in multimode systems. This is a general result that may imply that competing nonlinear effects can, at times, destroy existing nonlinear couplings. The paper describing the first observation of SSMC was chosen for the cover art for the March 2019 issue of *Optica* (Fig. 9). The multitude applications that can leverage this effect were covered in a patent[12].

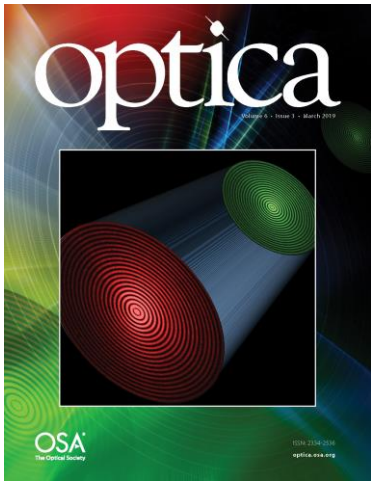

Fig. 9. Cover art in March 2019 issue of *Optica*.

5A) <u>SSMC applications: Time-locked multicolor ultrashort pulse sources:</u>

This new nonlinear scattering regime can be exploited for developing dual-color ultrafast sources for pump-probe dynamical studies in chemistry and biology. A crucial, rather obvious, requirement for such sources is that pulse at the two colors be spatio-temporally coincident, so as to maximize the interaction of the pump and probe with the material. Free-space bulk lasers can achieve this with careful beam alignment and delay arms, but in single-mode fibers, desired for remote, non-line-of-sight interrogation, the differing group-velocities of different colors along with the ultrashort (~100-fs) timescales, makes temporal alignment hard if not impossible. The SSMC process is *naturally* temporally aligned, since it initiates when the group-velocities in two different spatial modes are identical. If the process is stopped half-way during conversion, two colors that are naturally temporally locked as well as spatially coincident, are obtained[13]. Key results from this study are illustrated in Fig. 10.

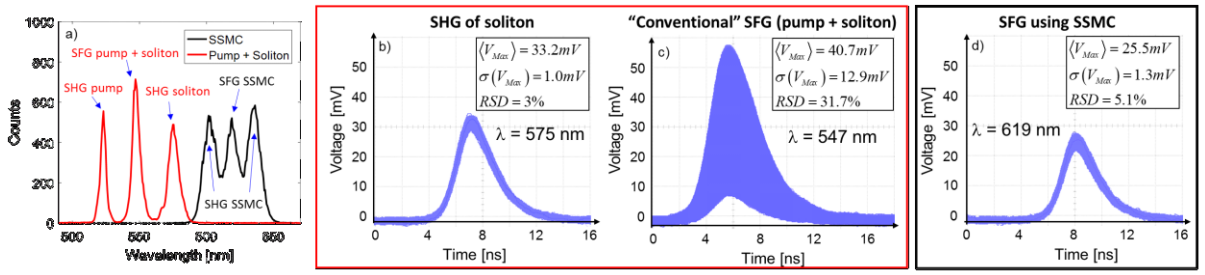

Fig. 10. (a) Spectra of generated second harmonic generation (SHG) and sum frequency generation (SFG) components for a conventional setup involving a pump and a distinct fiber soliton (called the pump + soliton) case, and for the SSMC pathway. (b)-(d) All three temporal figures display 20 second persistence traces. The calculated statistics provided along with each figure is the maximum peak value analyzed for 1000 pulses sampled over a few minutes. The two figures in the red box are for the conventional "pump + soliton" case, where (b) is SHG of the 1150 nm soliton and (c) is SFG between the pump and soliton. The figure in the black box (d) is SFG for the "SSMC" case. Hence, in contrast to dual-color emission from conventional fibers (pump+soliton case), two pulses from SSMC is substantially jitter free.

Given that two modes, when group-velocity matched across a Raman Stokes shift lead to dual color pulses, we investigated fiber designs in which this concept could be extended to when 3, or even 4 modes are similarly group-velocity matched. Indeed, upon finding such fiber designs, we are able to experimentally demonstrate a corresponding number of multi-color pulses that are temporally coincident at the fiber output. These results[14], depicted in Fig. 11, represent a variety of desirable attributes for multi-color ultrashort pulse sources: one can, by design, obtain a spectral comb of ultrashort pulses, and one can obtain dual-color sources of varying spectral separations, attractive for pump-probe experiments.

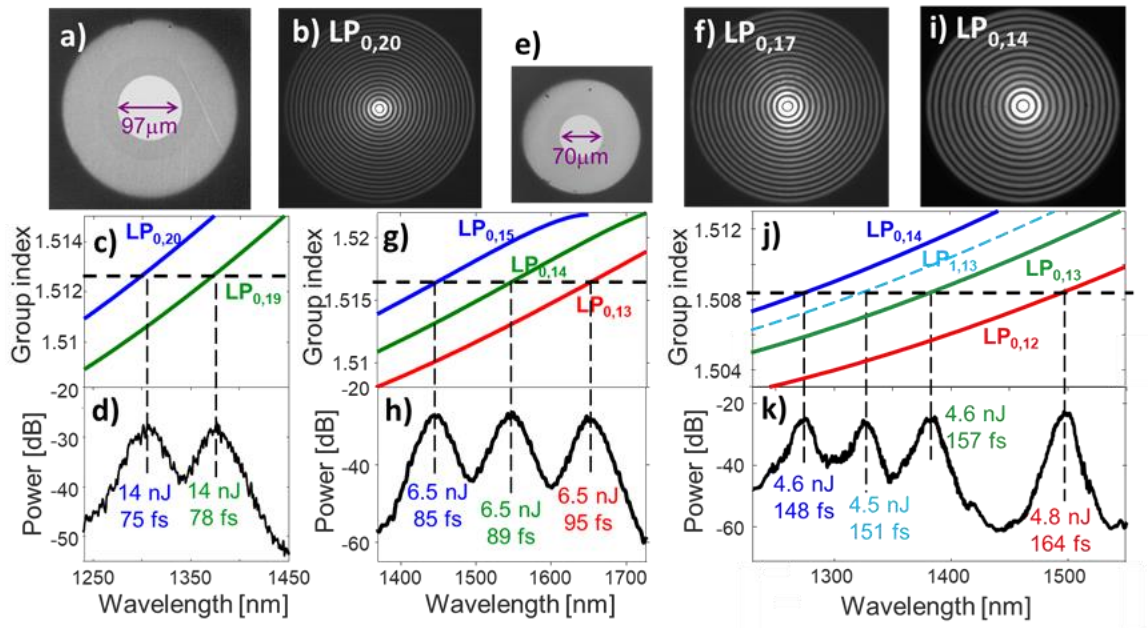

Fig. 11. (a), (e) Facet images of the two fibers used in the experiments. (b), (f), (i) Near field images of the pump modes used in the three experiments. (c), (g), (j) Group-index vs. wavelength for the modes participating in the three respective experiments. (d), (h), (k) the corresponding spectra of the multi-color emissions of the three experiments with pulse energies and autocorrelator-measured pulse widths shown for each peak. Vertical dashed lines show the excellent match between the experimentally observed spectral positions of the pulses, and the corresponding wavelengths at which the modes are group-velocity matched.

5B) SSMC applications: Nerve Imaging:

Leveraging the high energy ultrashort pulses now obtainable via the SSMC process described earlier, multiplexed multiphoton imaging becomes feasible. Figure 12 demonstrates[15] cross-sectional images of an axially frozen-sectioned human obturator nerve, with third-harmonic generation (THG) signal (Fig. 12a) from the myelin surrounding individual myelinated axons, and the SHG signal (Fig. 12b) from the collagen within the nerve sheath layers (i.e. endo-, peri-, and epineurium). In Fig. 12c the two images are merged to obtain a multicolor image of the peripheral nerve section. The combination of SHG and THG images reveal complementary information that permits characterization of nerve morphology in unstained tissues. The square and cubic power dependence of the SHG and THG signals were individually confirmed by measuring the emission as a function of the power of the excitation beam.

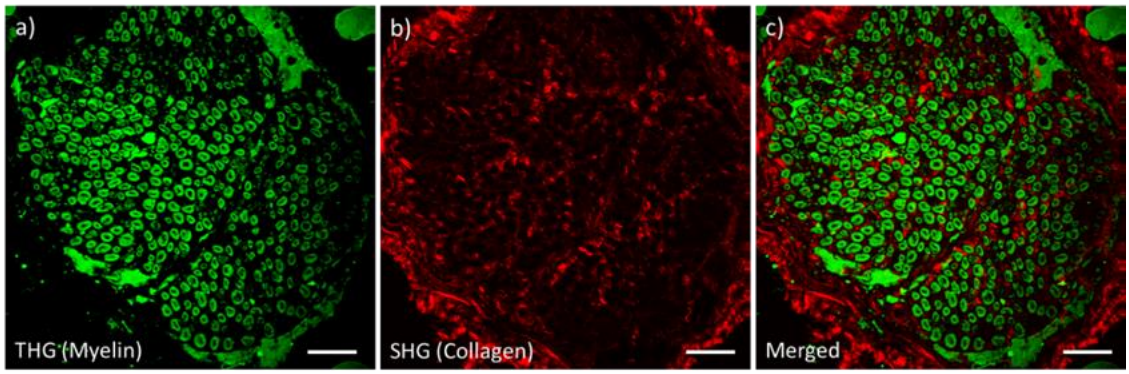

Fig. 12. Ex vivo label-free imaging of human obturator nerve. FOV is 380 x 380 µm and the scale bars are 50 µm. (a) THG signal of myelin fibers, (b) SHG image of collagen fibers, and (c) is the merged image.

The combination of SHG and THG imaging using a custom high-power single wavelength ultrafast fiber laser represents a novel means for label-free imaging of peripheral nerves. This approach may prove useful for assessment of peripheral nerve suitability for use in nerve transfer procedures. In addition, the robustness and alignment-free nature of the fiber laser makes it easily transferable to clinical settings, and furthermore, compatible with endoscopic applications.

6) Phase-Matched Raman Scattering due to Light's Chirality:

As a general rule, the strength of Raman scattering in an optical fiber scales as pump power and the inverse of mode area ($1/A_{eff}$), and is substantial, primarily for co-polarized pump and Stokes fields. Suppressing it involves strategies such as increasing A_{eff}, spectral filtering, operation away from the Raman emission band or cooling the fiber. Orbital angular momentum (OAM) modes of an optical fiber offer an additional degree of freedom that we show here to be very useful for suppressing Raman scattering *while* maintaining mode area, and hence all other linear and nonlinear attributes of the fiber mode that would be desired in applications.

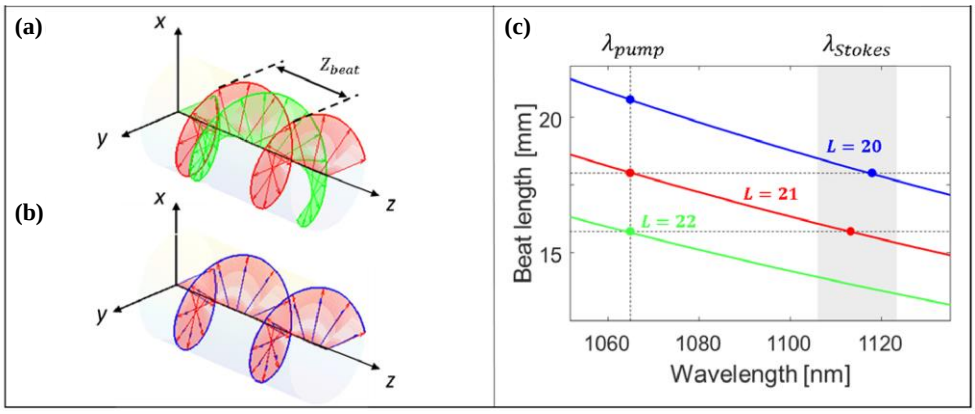

Fig. 13. Influence of chirality of modes on Raman scattering. (a, b) depict the polarization evolution of optically active OAM modes in fibers experiencing SOI. Red: Pump light in L_p=21, green: Stokes light in L_s=22, blue: Stokes light in L_s=20. Since polarization evolution beat lengths are a function of OAM topological charge L as well as wavelength (c), the polarization alignment of pump and Stokes light walks off for most modal combinations for this interaction (a), whereas it matches exactly for a certain wavelength pair for a specific combination of pump and Stokes and wavelengths (b).

Spin-orbit interaction (SOI), originating from the light-matter interaction at dielectric interfaces, splits the effective refractive index (Δn_{eff}) between $\hat{\sigma}^{\pm}$ states of same L, inducing optical activity (OA). As a result, the polarization orientation angle of linearly polarized light carrying OAM at the input of the fiber systematically rotates as it propagates, with the beat length $Z_{beat} = \lambda/\Delta n_{eff}$. Schematic plots of this polarization evolution are shown in Figs. 13(a) and 13(b). It is evident that Z_{beat} varies strongly with topological charge. In addition, waveguide dispersion makes Z_{beat} a strong function of wavelength too. Considering the Raman interaction, we can quantify the spatial frequency ($k = 2\pi/Z_{beat}$) difference of the linear polarization rotation between a pump and Stokes photon for arbitrary mode combinations as:

$$\Delta k = k_p - k_s = 2\pi\left[\frac{\Delta n_{eff}^{(p)}(\lambda_p)}{\lambda_p} - \frac{\Delta n_{eff}^{(s)}(\lambda_s)}{\lambda_s}\right] \quad (1)$$

where p and s represent pump and Stokes modes, respectively. When $\Delta k \neq 0$, which is the case for the majority of modes, Stokes light polarization walks off from the pump, as shown in Fig. 13(a). In contrast, as Fig. 13(b) illustrates, polarization rotation rates, and hence Z_{beat}, are matched, and hence $\Delta k = 0$, over narrow Stokes spectral ranges in the special case when Stokes light is in the mode order $L_s = L_p - 1$ [denoted by the horizontal dashed lines of Fig. 13(c)]. Hence, Raman scattering is restricted to this region, where the $\Delta k = 0$ condition is satisfied. This makes Stokes Raman scattering, normally considered to be a self-phase-matched process, dependent on phase matching, implying that Raman scattering strength as well as wavelength can be controlled by the topological charge of the pump.

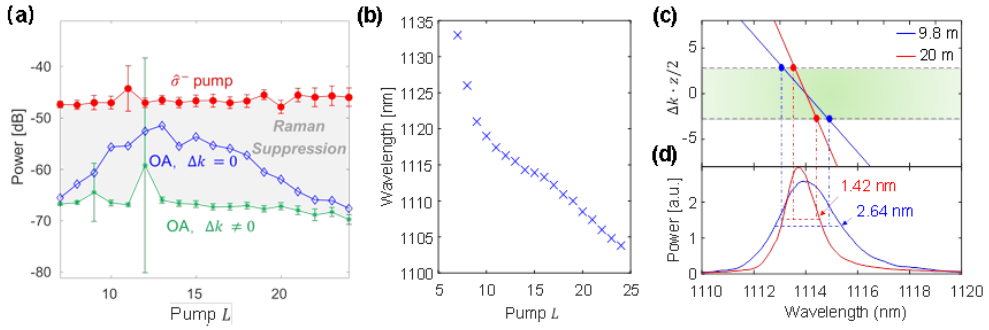

Fig. 14. (a) Integrated Raman power within 20 nm wavelength range for different pump-Stokes mode combinations, red: Raman power for {Stokes in $L_s, \hat{\sigma}^-$; Pump in $L_p, \hat{\sigma}^-$}; green: Raman power for $\{L_s \neq L_p - 1;\ L_p, \hat{x}\}$ combination, i.e. $\Delta k \neq 0$; blue: Raman power for $\{L_s = L_p - 1;\ L_p, \hat{x}\}$ combination, i.e. $\Delta k = 0$. Relatively larger error bars for some data points in red and green curves represent cases where a coincident, parasitic FWM peak existed, corrupting measurement of Raman power alone. (b) Peak wavelengths shift for Stokes mode in $L_s = L_p - 1$ as a function of pump mode $\{L_p, \hat{x}\}$. (c) Simulated plot of phase mismatch multiplied by fiber length as a function of wavelength for $\{L_s = 14; L_p = 15, \hat{x}\}$ mode combination. (d) Experimentally measured Raman spectral shape for $\{L_s = 14; L_p = 15, \hat{x}\}$ mode combination in both 9.8 and 20-m-long ring-core fibers.

Experimental demonstration[16] of this phenomenon is illustrated in Fig. 14. The red curve of Fig. 14(a) represents the co-polarized Raman scattering process where both pump and Stokes light are in the $\hat{\sigma}^-$ polarization, the flat trend with respect to L_p confirming conventional wisdom that Raman strength does not depend on the phases of the participating waves. In contrast, when the pump light is an optically active state arising from SOI, all but one of the Stokes modes experience phase mismatches due to non-zero Δk, and Stokes power is suppressed by ~ 20 dB, as illustrated

with the green curve of Fig. 14(a). For the Stokes mode corresponding to $L_s = L_p - 1$, we observe a systematic tunability of strength of Stokes power by over 15 dB since the Raman spectra are now tailored by the $\Delta k = 0$ condition [blue curve in Fig. 14(a)]. The spectral position of peak Raman gain now depends not only on the conventional Raman scattering strength of the material, but also its relation to the beat-length-matched wavelength λ_b. Figure 14(b) shows this new degree of freedom – the ability to tune the Raman gain peak wavelength λ_b, simply by tuning the topological charge of the pump mode, by over 30 nm (~ 8 THz), which is greater than half of the material's (Silica's) conventional Raman Stokes shift (~13 THz). Finally, Fig. 14(c) plots the simulated $\Delta k \cdot z/2$ values and Fig. 14(d) shows the corresponding experimentally recorded Raman spectra of $L_p = 15$; $L_S = 14$, for two different fiber lengths – $z = 9.8$m and 20m – shown in blue and red curves, respectively. The clear length dependence of spectral bandwidth of an otherwise self-momentum conserved scattering process illustrates the centrality of the role of phase matching Raman scattering, arising from SOI-induced chirality of the participating modes. This phenomenon may yield new methodologies for scaling the power of fiber lasers or for suppressing noise in fiber-based entangled photon pair generation.

7) OAM selection rules for Brillouin Scattering

The aforementioned distinct propagation behavior arising from SOI-induced chirality also plays a significant role in changing the dynamics of Stimulated Brillouin Scattering (SBS) in fiber modes[17]. In the case of circularly polarized OAM-carrying pumps $\mathcal{L}$; $\hat{\sigma}^{\pm}$, highly multimoded Stokes is observed, whose modal content is dictated by spatial overlap integrals (in analogy to the observed behavior from conventional fiber modes in standard fibers). In contrast, linearly polarized OAM pumps $\mathcal{L}$; $\hat{x}$ that experience chiral behavior exhibit dramatically different SBS

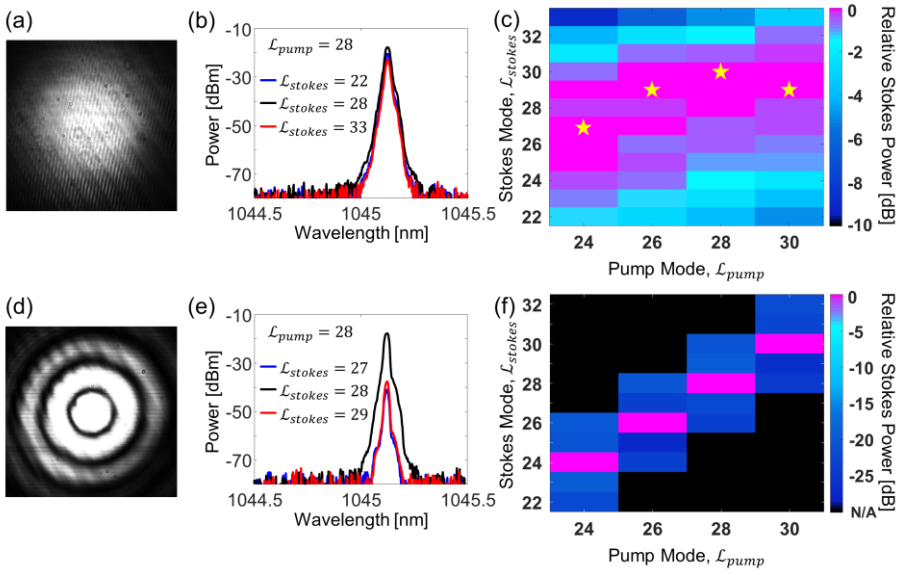

Fig. 4. (a,d) Far-field image, after an output mode sorter configuration of $\mathcal{L}_{mode-sorter} = -28$, of SBS Stokes light generated from a $\mathcal{L}_{pump} = 28$; $\hat{\sigma}^-$ and $\hat{x}$ pump, respectively, showing that, while the $\hat{\sigma}^-$ pump shows equipartitioning of Stokes power in several modes, with the $\hat{x}$ pump, all back-scattered Stokes resides in only the phase conjugated state relative to the pump. (b,e) Corresponding Stokes spectra illustrating the same contrasting behavior. (c,f) Matrix of relative Stokes powers for pumps of different $\mathcal{L}_{pump}$ with $\hat{\sigma}^-$ and $\hat{x}$ polarizations, respectively, showing that conventional equipartitioning of Stokes across modes occurs for all pump modes with $\hat{\sigma}^-$ polarizations, whereas pure phase conjugation is always observed with $\hat{x}$ polarized pumps, regardless of $\mathcal{L}_{pump}$.

behavior. Specifically, we see the rotational evolution of the polarization forces all Stokes light into a spatially phase conjugated state, suppressing other SBS interactions. Hence SBS behavior for each polarization state, circular and linear, differs from one another, in stark contrast to SBS behavior in conventional fibers, where it is agnostic to pump polarization state (Fig. 15). While spatial phase conjugation has long been known to occur for SBS, this is primarily in the context of an aberrated pump beam, whereas our experiments used stably propagating modes. OAM conservation laws also imply that the Stokes generated in these fibers are mediated by acoustic modes of record high OAM ($\mathcal{L}_A = 63$). In general, we show that the angular momentum content of light plays a critical role in controlling the strength, modal content and frequency of the Stokes light, and hence represents an alternative toolbox with which SBS can be controlled in optical fibers.

8) Other work

Over the period of performance of this program, we also engaged in several other smaller efforts that were complementary to, or building blocks for, the aforementioned seven key results:

a) Versatile techniques for mode excitation in optical fibers[18].

b) Multimode pumped Raman lasers operating in higher order modes[19].

c) Experimental verification of the spin-orbit coupling effect because of OAM in optical fibers[20].

d) The effect of index contrast on the polarization structure of fiber eigenmodes[21].

e) Fiber designs that can enhance mode stability.[22]

f) Demonstration of Silicon optical fibers[23].

g) Dispersion control using transmissive long-period fiber gratings[24].

References

[1] J. Demas, P. Steinvurzel, B. Tai, L. Rishøj, Y. Chen, and S. Ramachandran, "Intermodal nonlinear mixing with Bessel beams in optical fiber," Optica 2, 14 (2015).

[2] J. Demas, G. Prabhakar, T. He and S. Ramachandran, "Wavelength-agile high-power sources via four-wave mixing in higher-order fiber modes," Opt. Exp. 25, 7455(2017).

[3] X. Liu, E.N. Christensen, K. Rottwitt and S. Ramachandran, "Nonlinear four-wave mixing with enhanced diversity and selectivity via spin and orbital angular momentum conservation," APL Photonics 5, 010802 (2020).

[4] J. Demas, L. Rishøj, X. Liu, G. Prabhakar, S. Ramachandran, "Intermodal group-velocity engineering for broadband nonlinear optics," Photon. Res. 7, 1-7 (2019).

[5] G. Prabhakar, P. Gregg, L. Rishoj, P. Kristensen, and S. Ramachandran, "Octave-wide supercontinuum generation of light-carrying orbital angular momentum," Opt. Express 27, 11547-11556 (2019).

[6] A.P. Greenberg, G. Prabhakar, and S. Ramachandran, "High resolution spectral metrology leveraging topologically enhanced optical activity in fibers," Nature Communications 11, 5257 (2020).

[7] Siddharth Ramachandran, Gautam Prabhakar, Aaron Greenberg, "Engineered optical fibers and uses thereof," US patent 10823667.

[8] L. Rishøj, B. Tai, P. Kristensen, and S. Ramachandran, "Soliton self-mode conversion: revisiting Raman scattering of ultrashort pulses," Optica 6, 304-308 (2019).

[9] A. Antikainen, L. Rishøj, B. Tai, S. Ramachandran, and G. P. Agrawal, “Fate of a Soliton in a High Order Spatial Mode of a Multimode Fiber,” Phys. Rev. Lett. 122, 023901 (2019).

[10] H.B. Kabagöz, A. Antikainen and S. Ramachandran, "Converting noise into solitons: optical self-organization through intermodal nonlinearity," Opt. Express 29, 18315-18324 (2021).

[11] A. Antikainen, H B. Kabagöz, and S. Ramachandran, “Fragility of a soliton’s shot-to-shot coherence,” Opt. Lett. 45, 5393 (2020).

[12] Siddharth Ramachandran, Lars Rishoj, Jeffrey Demas, “Ultrashort Pulse Fiber Laser Employing Raman Scattering in Higher Order Mode Fibers” US Patent 10734782

[13] L. Rishøj, F. Deng, B. Tai, J-X. Cheng, and S. Ramachandran, "Jitter-free, dual-wavelength, ultrashort-pulse, energetic fiber sources using soliton self-mode conversion," Opt. Express 28, 4333-4339 (2020)

[14] H.B. Kabagöz, A. Antikainen, and S. Ramachandran, “Passive, controllable generation of energetic multi-color pulses via spatial mode re-organizations in optical fibers,” APL Photonics 6, 126109 (2021).

[15] L. Rishøj, I.C. Hernández, S. Ramachandran, N. Jowett, N, “Multiphoton microscopy for label-free multicolor imaging of peripheral nerve,” Journal of Biomedical Optics 27, 056501 (2022).

[16] X. Liu, Z. Ma, A. Antikainen, S. Ramachandran, “Raman gain control in optical fibers with orbital-angular-momentum-induced chirality of light,” Opt. Express 30, 26967-26974 (2022)

[17] A.P. Greenberg, Z. Ma, and S. Ramachandran, "Angular momentum driven dynamics of stimulated Brillouin scattering in multimode fibers," Opt. Express 30, 29708-29721 (2022)

[18] J. Demas, L. Rishøj and S. Ramachandran, “Free-space beam shaping for precise control and conversion of modes in optical fiber,” Opt. Exp. 23, 28531 (2015).

[19] S. Zhu, S. Pidishety, Y. Feng, S. Hong, J. Demas, R. Sidharthan, S. Yoo, S. Ramachandran, B. Srinivasan, J. Nilsson, "Multimode-pumped Raman amplification of a higher order mode in a large mode area fiber," Opt. Express 26, 23295-23304 (2018).

[20] D.L.P. Vitullo, C.C. Leary, P. Gregg, R.A. Smith, D.V. Reddy, S. Ramachandran and M. G. Raymer, “Observation of Interaction of Spin and Intrinsic Orbital Angular Momentum of Light," Phys. Rev. Lett. 118, 083601 (2017).

[21] L. Rishøj, M. Jones, J. Demas, P. Gregg, G. Prabhakar, L. Yan, T. Hawkins, J. Ballato, and S. Ramachandran, "Polymer-clad silica fibers for tailoring modal area and dispersion," Opt. Lett. 41, 3587-3590 (2016).

[22] A. Gulistan, S. Ghosh, S. Ramachandran, and B.M.A. Rahman, "Efficient strategy to increase higher order inter-modal stability of a step index multimode fiber," Opt. Express 25, 29714 (2017)

[23] M. Ordu, J. Guo, B. Tai, M.K. Hong, S. Erramilli, S. Ramachandran and S.N. Basu, "Mid-infrared transmission through germanium-core borosilicate glass-clad semiconductor fibers," Opt. Mater. Express 7, 3107-3115 (2017).

[24] T. He, J. Demas and S. Ramachandran, "Ultra-low loss dispersion control with chirped transmissive fiber gratings," Opt. Lett. 42, 2531-2534 (2017).